Ultramicroscopy 111 (2011) 1352–1359

Contents lists available at ScienceDirect

Ultramicroscopy

journal homepage: www.elsevier.com/locate/ultramic

A method to determine the local surface profile from reconstructed exit waves

A. Wang [a,*], F.R. Chen [b], S. Van Aert [a], D. Van Dyck [a]

[a] Department of Physics, University of Antwerp, Groenenborgerlaan 171, 2020 Antwerp, Belgium
[b] National Tsing Hua University, Department of Engineering and System Science, No. 101, Sec.2, Kuang-Fu Road, 300 Hsinchu, Taiwan

ARTICLE INFO

Article history:
Received 19 November 2010
Received in revised form
19 April 2011
Accepted 24 April 2011
Available online 1 May 2011

Keywords:
Defocus
Electron scattering
Channelling theory
Crystalline structure
Image simulation

ABSTRACT

Reconstructed exit waves are useful to quantify unknown structure parameters such as the position and composition of the atom columns at atomic scale. Existing techniques provide a complex wave in a flat plane which is close to the plane where the electrons leave the atom columns. However, due to local deviation in the flatness of the exit surface, there will be an offset between the plane of reconstruction and the actual exit of a specific atom column. Using the channelling theory, it has been shown that this defocus offset can in principle be determined atom column-by-atom column. As such, the surface roughness could be quantified at atomic scale. However, the outcome strongly depends on the initial plane of reconstruction especially in a crystalline structure. If this plane is further away from the true exit, the waves of the atom columns become delocalized and interfere mutually which strongly complicates the interpretation of the exit wave in terms of the local structure. In this paper, we will study the delocalization with defocus using the channelling theory in a more systematic way.

1. Introduction

High resolution electron microscopy exit waves often show a one-to-one correspondence with the configuration of projected atom columns when a crystal is viewed along a zone-axis. The physical reason for the local nature of the dynamical scattering is the channelling of the electrons along the atom columns parallel to the beam direction. This can be described on an intuitive basis by means of the channelling theory [1–3]. This theory expresses the exit wave in a simple closed-form equation that can be used for further quantitative refinement of structure parameters such as the positions and the "weight" of the atom columns [4,5]. Furthermore, the protrusion of atom columns at the surfaces can be detected and even quantified for every atom column [6].

In practice, a series of through-focal images [7–10] or an off-axis hologram [11] is used to reconstruct an exit wave in a flat plane close to the plane where the electrons leave the atom columns. However, one does not know beforehand exactly at which plane the exit wave is reconstructed. Moreover, due to local deviations in the surface flatness, an ideal exit wave does not exist but there will be an offset between the plane of reconstruction and the actual exit of a specific atom column. In other words, the exact defocus of each atom column is unknown. In [6], it has been shown that this offset can in principle be determined atom column-by-atom column using the channelling theory applied to isolated columns. In addition, this theory works well for simulations of wedge shaped structures in which the simulated exit waves are close to the true exit of the atom columns. However, in experimental exit wave reconstructions, the initial plane of reconstruction is unknown and also the influence of neighboring columns needs to be taken into account. If this initial plane is further away from the true exit, the waves of the atom columns indeed become delocalized and interfere mutually which complicates the interpretation of the exit wave in terms of the local structure. In very specific cases, the electron wave can reappear periodically for certain focus values, which is the origin of so-called Fourier images [12]. Therefore, we will show how to determine the defocu1s in crystalline structures in this paper in a more systematic way. This approach will also provide an intuitive view of the wave physics behind Fourier images.

The content of this paper is as follows: in Section 2, the channelling theory will be summarized and the defocus of the exit wave will be included. In Section 3, the effect of neighboring columns on the exit wave will be described. In Section 4, the results will be summarized.

2. Theory

In this section, the effect of defocus on the exit wave will be investigated using the channelling theory [1–3,13]. The main concept of the theory is briefly summarized here. When a crystal is in a low-order zone-axis direction, the atoms are aligned in atom columns and the distance between the atom columns is large enough to avoid overlapping of the column states. Due to the

* Corresponding author. Tel.: +32 3 2653252; fax: +32 3 2653318.
E-mail address: amy.wang@ua.ac.be (A. Wang).

0304-3991/$ - see front matter © 2011 Elsevier B.V. All rights reserved.
doi:10.1016/j.ultramic.2011.04.005

electrostatic potential of the atoms, the incoming electrons scatter dynamically without leaving the atom columns. An intuitive way of describing this is to consider atoms as lenses so that the electron wave is focused at periodic distances, the so-called extinction distance. The channelling theory uses a basis of eigenstates of the Hamiltonian of the projected electrostatic column potential which leads to a simple closed-form expression for the exit wave. The channelling equation can be regarded as a solution of the time-dependent Schrödinger equation assuming the incoming electrons to be at constant speed so that the depth is proportional to the time. For an isolated atom column, the exit wave can be expressed mainly by the lowest bound state, the *s*-state, as [13]

$$\psi(\mathbf{r},z)=1+c_s\phi_s(\mathbf{r}-\boldsymbol{\beta})\left[\exp\left(-i\pi\frac{E_s}{E_0}\frac{1}{\lambda}z\right)-1\right] \tag{1}$$

assuming the incident wave to be equal to 1 (plane wave). The second term on the right-hand side of Eq. (1) represents the interaction wave, with $\mathbf{r}$ a two-dimensional vector in the plane perpendicular to the incoming electron beam direction, E_0 the beam energy, λ the wavelength and z the thickness. The symbol E_s is the eigenenergy of the *s*-state function $\phi_s(\mathbf{r}-\boldsymbol{\beta})$, which is peaked at the column position $\boldsymbol{\beta}=(\beta_x,\beta_y)$. From [13], the *s*-state function may be approximated by a quadratically normalized and parameterized Gaussian function with column dependent width a

$$\phi_s(\mathbf{r}-\boldsymbol{\beta})=\frac{1}{a\sqrt{2\pi}}\exp\left(-\frac{(\mathbf{r}-\boldsymbol{\beta})^2}{4a^2}\right). \tag{2}$$

The excitation coefficient c_s is given by

$$c_s=2\sqrt{2\pi}a. \tag{3}$$

An Argand plot is a convenient way to visualize the structure information encoded in the complex exit wave [3,6,14–16]. An Argand plot is a complex plane where the *x*- and *y*-axes correspond to the real and imaginary parts of the complex pixel value, respectively. When applied to complex electron exit waves, the pixel values are taken at the estimated atom column position. In [6], it was shown that the position in an Argand plot depends on the mass of the atom column and the absorption resulting from phonon scattering. For atom columns with different mass (e.g. atom columns with the same type of atoms but with different numbers of atoms in the columns), the complex pixel values follow a circular locus with the angle proportional to the mass of the atom column.

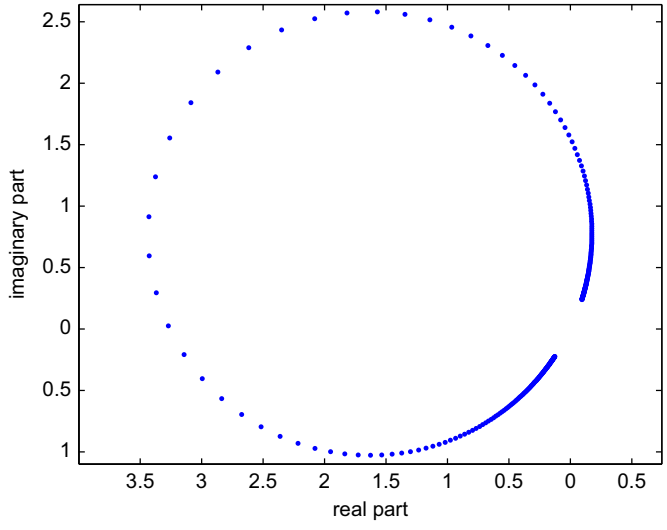

Fig. 1. The defocus circle for a simulated Au[1 0 0] single atom column based on the channelling theory. The atom column contains five Au atoms with interatomic distance equals to 4 Å. The exit wave was defocused from −400 to +400 Å with a defocus step of 2 Å.

When absorption is present, the circular locus becomes a logarithmic spiral. Furthermore, the positions of the complex pixel values in the Argand plot are strongly influenced by the defocus, that is, the distance from the actual exit positions of the atom columns to the exit wave plane. The defocus effect of an atom column can be described by convoluting Eq. (1) with the defocus propagator $p(\mathbf{r})$, of which the two-dimensional Fourier transform is given by

$$P(\mathbf{g})=\exp(-i\pi\varepsilon\lambda\mathbf{g}^2), \tag{4}$$

where ε is the defocus distance. Using the convolution theorem, the defocused wave for an atom column then becomes

$$\psi(\mathbf{r},z)=1+\frac{8\pi a^2}{4\pi a^2+i\varepsilon\lambda}\exp\left(-\frac{(\mathbf{r}-\boldsymbol{\beta})^2}{4a^2+i\frac{\varepsilon\lambda}{\pi}}\right)\left[\exp\left(-i\pi\frac{E_s}{E_0}\frac{1}{\lambda}z\right)-1\right]. \tag{5}$$

A series of exit waves, defocused from −400 to +400 Å with a defocus step of 2 Å, has been simulated using Eq. (5) for a Au[1 0 0] single atom column containing five atoms. The interatomic distance is 4 Å. Parameters a and E_s are 0.13 Å and −210.8 eV, respectively (see [17]). The incident beam energy E_0 used is 300 keV. Throughout this paper, the structure and microscope parameters are the same unless otherwise specified. The complex pixel values for every defocused exit wave at the column position is as shown in Fig. 1 in the form of an Argand plot. On defocusing, the point follows a circular curve, the *defocus circle*, as proven in [6]. It was concluded that, for every atom column, one can accurately calculate the defocus value of every atom column from its defocus circle provided the zero-defocus point is known. As such, the surface structure at the exit surface can be retrieved. However, neighboring columns have a significant effect on the defocus circle. Indeed, when the defocus becomes larger, the exit waves of the neighboring columns become more delocalized and start overlapping. This is shown in Figs. 2 and 3. The figures show the profiles of the amplitude and the phase part of the defocused waves from the first neighboring columns located 2 Å from the center. It is clearly shown that for a defocus value up to −20 Å the neighboring column waves have little effect at the center. As the defocus value increases, the wave at the center significantly interferes with the neighboring column waves. Therefore, it is important to study their effect in more detail and to show how the defocus can be accurately determined even in the presence of neighboring columns. Note that in this study, the distance between two atom columns is 2 Å. In [18], it was shown that even for smaller distances, the exit wave can still be expressed as an expansion of the *s*-state waves. Even for closely spaced columns like in GaN[1 1 0], for which the distance between columns in a dumbbell is only 1.13 Å, the *s*-state model is still sufficient for thicknesses up to 9 nm.

3. Effect of neighboring columns on the defocus circle

In this section, we will focus on the effects of neighboring columns on the defocus circle. Therefore, we will only consider the defocus part of the interaction wave in Eq. (5):

$$\varphi(\mathbf{r}-\boldsymbol{\beta})=\frac{8\pi a^2}{4\pi a^2+i\varepsilon\lambda}\exp\left(-\frac{(\mathbf{r}-\boldsymbol{\beta})^2}{4a^2+i\frac{\varepsilon\lambda}{\pi}}\right). \tag{6}$$

The amplitude and phase part of Eq. (6) are, respectively,

$$amp(\varphi)=\frac{8\pi a^2}{\sqrt{(4\pi a^2)^2+(\varepsilon\lambda)^2}}\exp\left(-\frac{(\mathbf{r}-\boldsymbol{\beta})^2 4a^2}{(4a^2)^2+\left(\frac{\varepsilon\lambda}{\pi}\right)^2}\right) \tag{7}$$

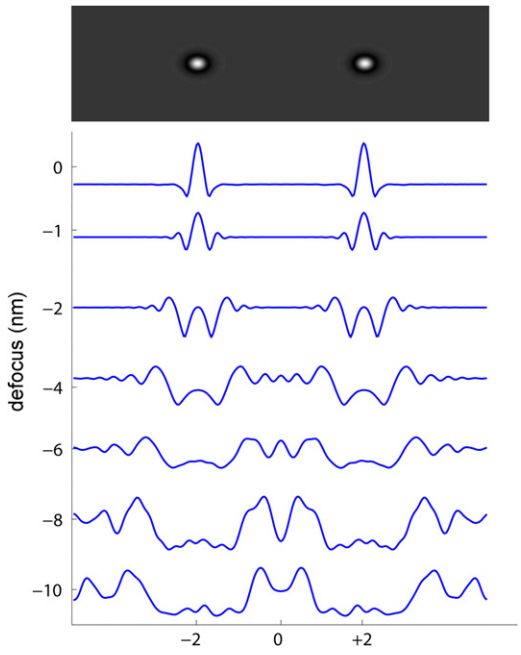

Fig. 2. The profiles of the amplitude of the defocused waves from the first neighboring columns located 2 Å from the center (0). The image of the amplitude part for the on-focus wave is shown on the top.

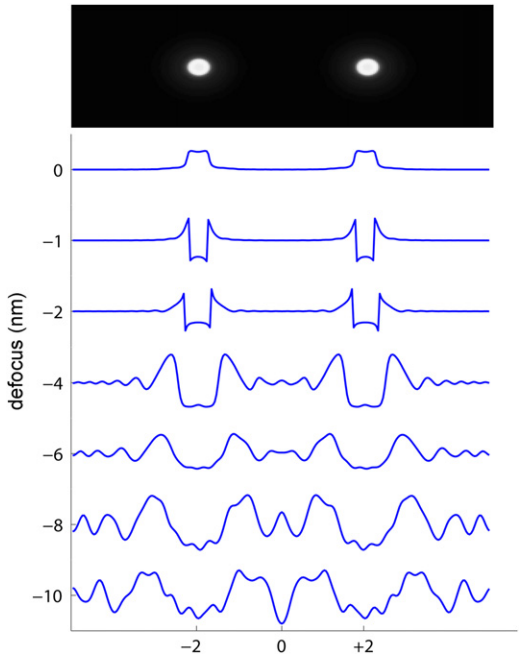

Fig. 3. The profiles of the phase of the defocused waves from the first neighboring columns located 2 Å from the center (0). The image of the phase part for the on-focus wave is shown on the top.

and

$$arg(\varphi)=\tan^{-1}\left(-\frac{\varepsilon\lambda}{4\pi a^2}\right)+\left(\frac{(\mathbf{r}-\boldsymbol{\beta})^2\frac{\varepsilon\lambda}{\pi}}{(4a^2)^2+\left(\frac{\varepsilon\lambda}{\pi}\right)^2}\right). \tag{8}$$

Next, the effect of neighboring columns will be taken into account by adding their contributions to the center column under study. Let us assume that neighboring columns have the same columnar structure as the center column which is set at $\boldsymbol{\beta}=(0,0)$. Then it follows from Eq. (6) that all contributions to the center column are given by the following expression:

$$\varphi(\mathbf{0})=\frac{8\pi a^2}{4\pi a^2+i\varepsilon\lambda}\left(1+\sum_{j=1}^{n}\exp\left(-\frac{\delta_j^2}{4a^2+i\frac{\varepsilon\lambda}{\pi}}\right)\right), \tag{9}$$

where δ_j is the distance from the center to the jth neighboring column. Eq. (9) will now be evaluated for small and large defocus values.

Small defocus:

$$\frac{\varepsilon\lambda}{\pi}\ll 4a^2. \tag{10}$$

Then Eq. (6) becomes

$$\varphi(\mathbf{r})=\frac{8\pi a^2}{4\pi a^2+i\varepsilon\lambda}\exp\left(-\frac{(\mathbf{r}-\boldsymbol{\beta})^2}{4a^2}\right) \tag{11}$$

and Eq. (9) becomes

$$\varphi(\mathbf{0})=\frac{8\pi a^2}{4\pi a^2+i\varepsilon\lambda}\left(1+\sum_{j=1}^{n}\exp\left(-\frac{\delta_j^2}{4a^2}\right)\right). \tag{12}$$

The width a of the s-state dominates over the defocus term $\varepsilon\lambda/\pi$. The wavefunction is thus sharply peaked at the central atom column position. If the distance between two atom columns is larger than the width a, the contribution of the wave function of the adjacent columns to the central column is negligible. As a result, the defocus curve follows a circle.

Large defocus:

$$\frac{\varepsilon\lambda}{\pi}\gg 4a^2. \tag{13}$$

Then Eq. (6) becomes

$$\varphi(\mathbf{r})=\frac{8\pi a^2}{4\pi a^2+i\varepsilon\lambda}\exp\left(-\frac{(\mathbf{r}-\boldsymbol{\beta})^2}{i\frac{\varepsilon\lambda}{\pi}}\right) \tag{14}$$

and Eq. (9) becomes

$$\varphi(\mathbf{0})=\frac{8\pi a^2}{4\pi a^2+i\varepsilon\lambda}\left(1+\sum_{j=1}^{n}\exp\left(-\frac{\delta_j^2}{i\frac{\varepsilon\lambda}{\pi}}\right)\right). \tag{15}$$

In this regime, the defocus term dominates over the width of the s-state. Neighboring columns cause the defocus curve to follow a spiral-like curve which strongly depends on the distance of the neighboring atom column, or more generally, on the configuration of the lattice structure.

In Fig. 4(a), the influence of the first neighboring columns, which are set at 2 Å away from the center atom column, is shown. In order to compare these results with multislice simulations, the incident wave 1 and the thickness dependent term $[\exp(-i\pi(E_s/E_0)(1/\lambda)z)-1]$ have been taken into account whereas the center atom column contribution has been neglected. Note that due to lattice symmetry, there are four neighboring columns with identical contributions. As expected, the contribution is small for small defocus values. Thus the points are close to the value of the entrance wave corresponding to (1,0). As the defocus value increases, the points follow a spiral-like curve. In Fig. 4(b), a similar calculation is shown using the multislice theory [19].

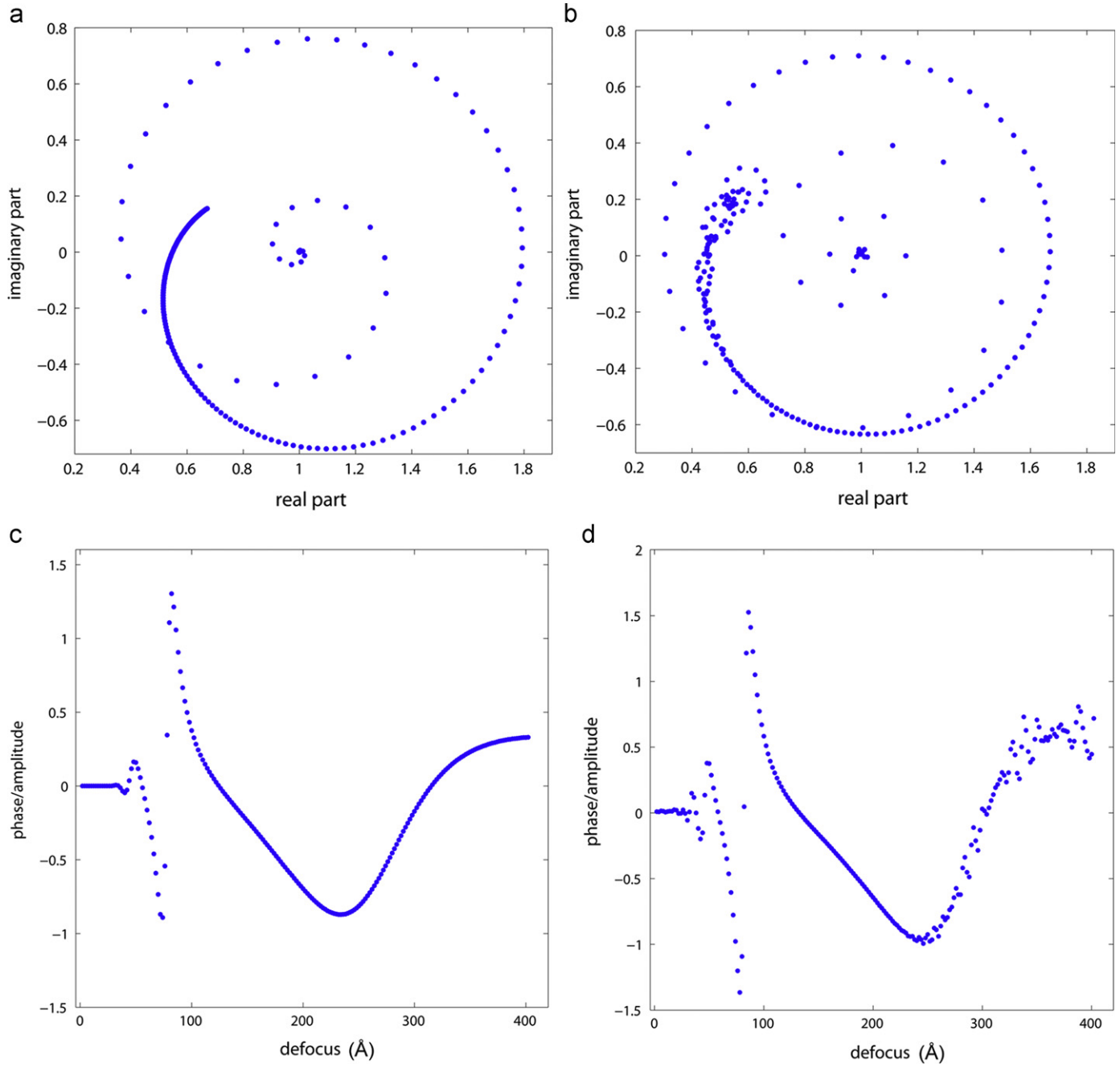

Fig. 4. Simulations of the influence of the first neighboring columns which are set at a distance of 2 Å from the center atom column. (a) and (b) are the influences according to the channelling theory and multislice theory, respectively. (c) and (d) are the ratio of phase to amplitude from the (a) and (b) curves, respectively.

By comparing this figure with Fig. 4(a), it follows that both curves behave very similarly. In addition, in (c) and (d), the ratios of phase to amplitude from (a) and (b) curves are plotted. Again, the influence is small for small defocus values whereas there is a linear relationship between phase and amplitude for larger defocus values, roughly between 100 and 200 Å. The linear relationship follows from the exponential term and the arctangent term in Eqs. (7) and (8), respectively. For even larger defocus values, the waves are strongly delocalized such that all structure information is mixed. The wave in a sense approaches a plane wave function explaining the convergence of the defocus curve to a stationary point.

In Fig. 5 the effects of first, second and third neighboring columns are simulated with the Au parameters using Eq. (9). The projected structure is illustrated in Fig. 5(a) with the atom column distance equal to 2 Å. The waves are defocused from -400 to $+400$ Å. Fig. 5(b)–(d) shows the effects of the first, second and third neighbors separately, with the distance from the center column equal to 2, $2\sqrt{2}$ and 4 Å, respectively. The dots represent the defocus circle as in a single isolated atom column case while the arrows represent the amplitude and phase change of the dots influenced by neighboring columns. As expected, the closer the neighboring columns, the stronger the influence on the defocus circles. Fig. 5(e) shows the total effect of all neighboring columns up to third order. If the absolute defocus value increases, the trace of the defocus curve starts to follow another circular curve. For even larger absolute defocus values, the curve oscillates and circles around the background wave, which is 0 in this simulation.

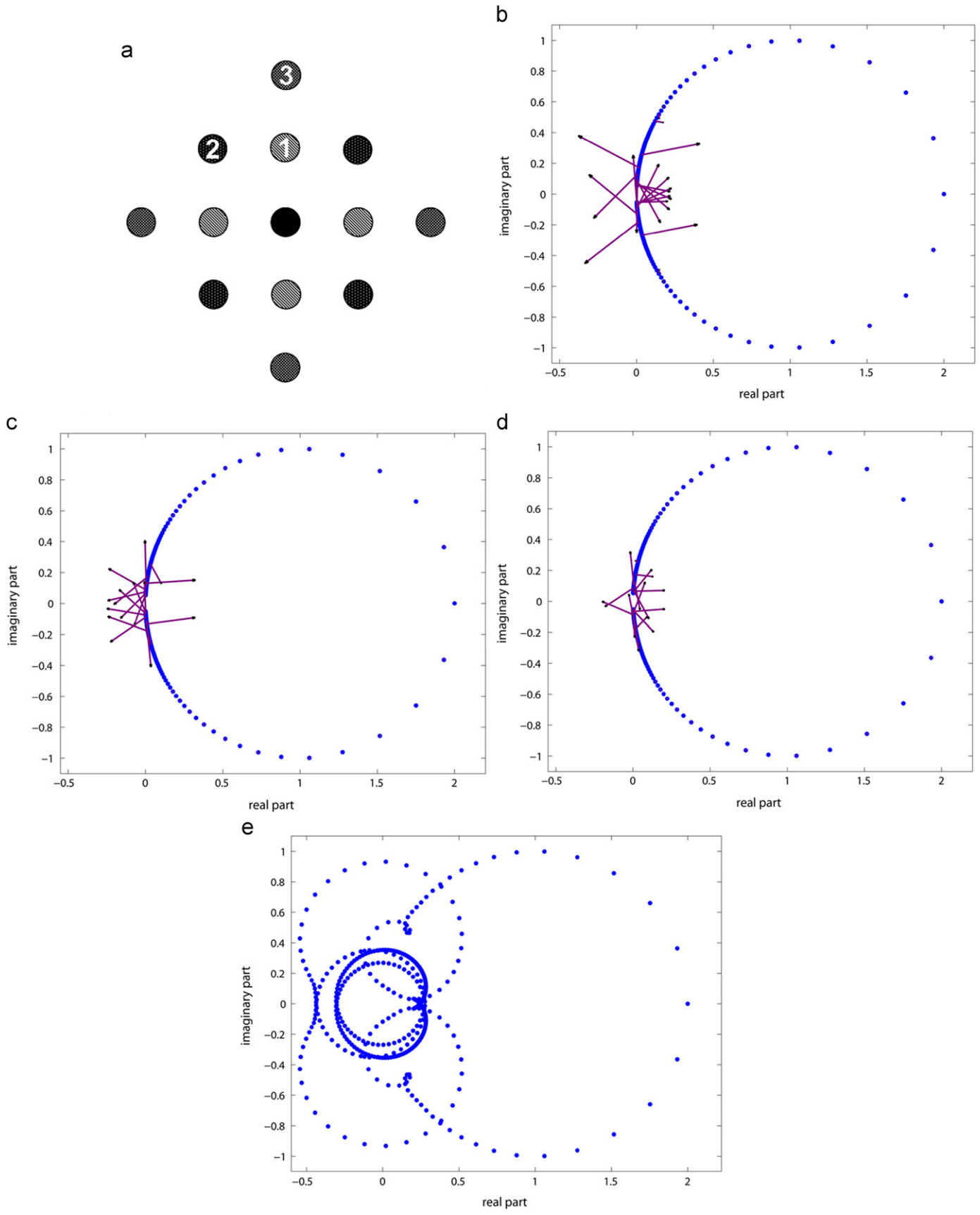

Fig. 5. Simulations of neighboring columns according to the channelling theory using Eq. (9). (a) The projected structure. Every atom column is identical and the distance between two columns is 2 Å. The wave is defocused from -400 to $+400$ Å with a defocus step of 2 Å. (b), (c) and (d) show the effects of the 1st(2 Å), 2nd ($2\sqrt{2}$ Å) and 3rd (4 Å) closest neighbors, respectively. The dots represent the defocus circle as in a single atom column case using Eq. (6) with $\mathbf{r}=\mathbf{0}$. The arrows represent the amplitude and phase change of the position of the dots influenced by neighboring columns. (e) The total effect of the first three neighboring columns.

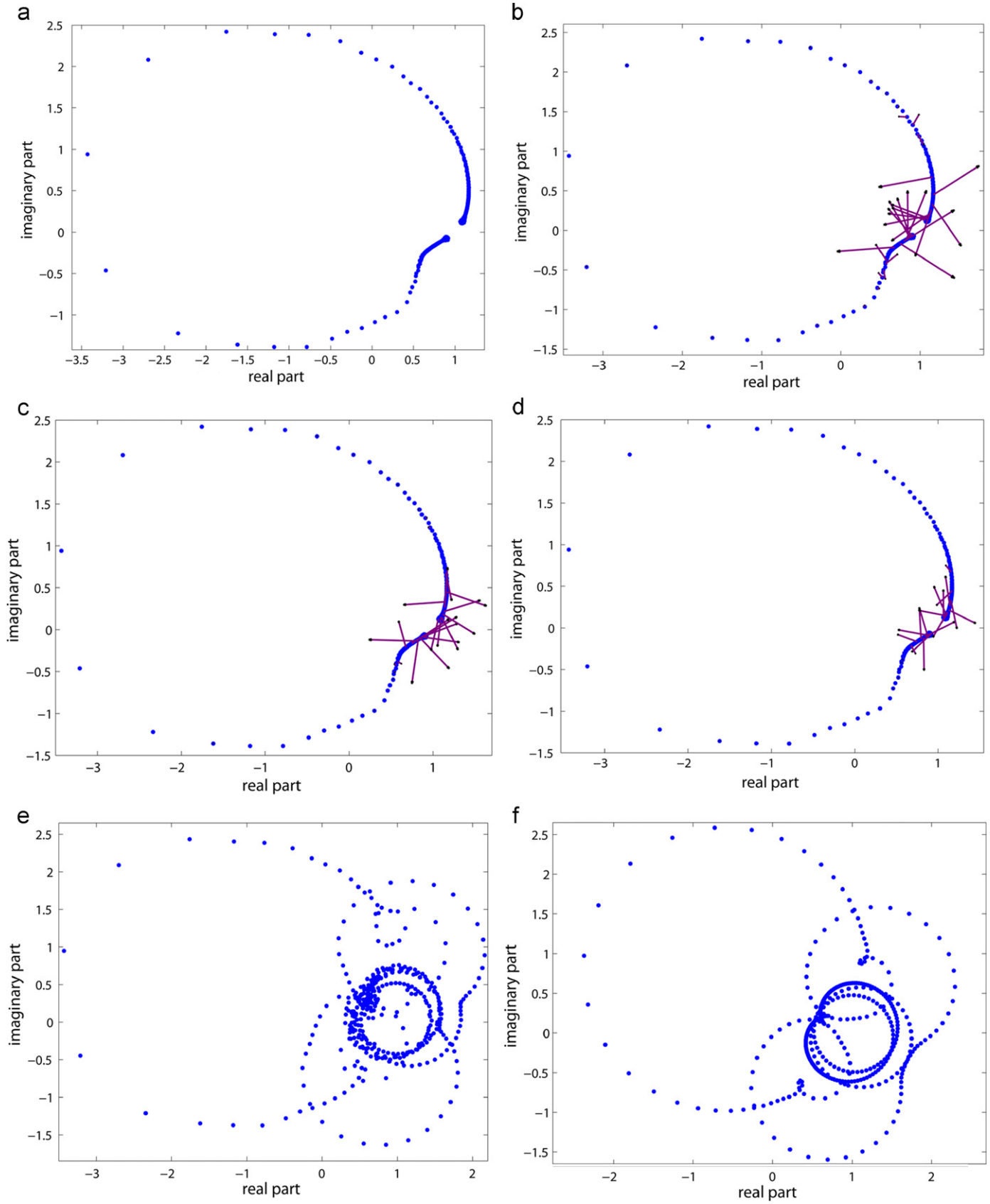

Fig. 6. Simulations of the exit waves with neighboring columns according to the multislice theory. (a) The defocus curve for a single Au atom column with five atoms in the column. The interatomic distance is 4 Å. The exit wave was defocused from −400 to +400 Å with defocus step 2 Å. As in Fig. 5, (b)–(d) show the effects of the 1st, 2nd and 3rd closest neighbors, respectively. The dots represent the same defocus curve as in (a) while the arrows show the amplitude and phase change influenced by the neighboring columns. (e) The total effect of the first three neighboring columns. (f) Simulation of the exit wave based on the channelling theory for comparison with (e).

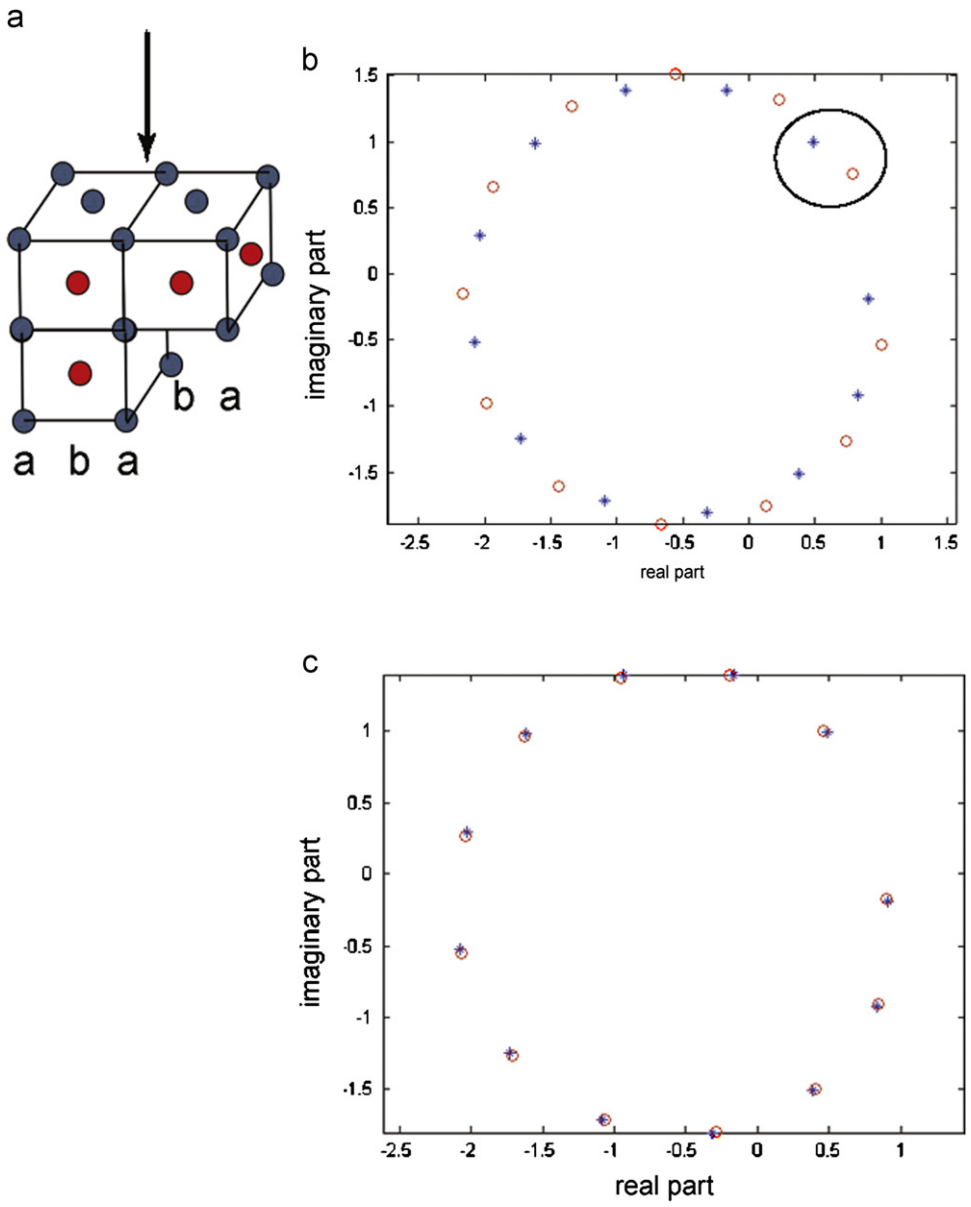

Fig. 7. Simulations of neighboring columns with different heights along the beam direction. (a) The crystal structure of the *a* and *b* columns where the *b* columns are vertically displaced by half a lattice parameter in the beam direction. (b) The Argand plot for the *a* (∗) and the *b* (○) columns. The neighboring dots, as circled, are *a* and *b* columns with the same number of atoms. The circles on the Argand plot for both columns are rotated relatively to each other. (c) By shifting the potential over half a unit cell, the dots for the *b* columns overlap with the *a* columns.

An important conclusion following from these results is that there is no effect on the defocus circle in the range close to the zero-defocus point. In this Au simulation, there is indeed no effect in the defocus range from -20 to $+20$ Å. For comparison, multislice calculations are shown in Fig. 6. Note that in these multislice calculations, the thickness dependent factor cannot be neglected. Fig. 6(f) shows a simulation using the channelling theory including the thickness dependent factor. It is clearly shown that also in the defocus range close to the zero-defocus point, the defocus circle is unaffected. It can thus be concluded that for small defocus, the wave is still dominated by the *s*-state of the atom column. A simple rule of thumb for this defocus range can be derived as follows. As mentioned in Section 2, the defocus effect of an atom column can be described by convoluting $\psi(\mathbf{r},z)$ with the propagator

$$\psi(\mathbf{r},z) = \int \psi(\mathbf{g})\exp(2\pi i\mathbf{g}\cdot\mathbf{r})\exp(i\pi\varepsilon\lambda g^2)\,d\mathbf{g} \tag{16}$$

$$= \int \psi(\mathbf{g})\exp\left(2\pi i\mathbf{g}\cdot\left(\mathbf{r}+\frac{1}{2}\varepsilon\lambda\mathbf{g}\right)\right)d\mathbf{g}, \tag{17}$$

where $\psi(\mathbf{g})$ is the wave function in Fourier space. Thus, on defocusing over ε, the contribution of a particular spatial frequency g is given by $\varepsilon\lambda g/2$. Assuming that this delocalization should be smaller than half the distance between the atom columns δ then yields

$$\frac{\varepsilon\lambda g}{2} < \frac{\delta}{2}. \tag{18}$$

The maximum spatial frequency is related to the resolution ρ as $g_{max} = 1/\rho$, so that we obtain

$$\varepsilon < \frac{\delta\rho}{\lambda}. \tag{19}$$

For $\lambda = 0.02$ Å (300 keV), $\rho = 0.15$ Å and $\delta = 2$ Å (Au), we then obtain $\varepsilon < 15$ Å. This is comparable to the simulation case, $\varepsilon \leq 20$ Å, in which only the first three neighboring columns are

included. Moreover, the maximum surface roughness that can be obtained can be estimated from Eq. (19):

$$\tan\theta_r = \frac{\varepsilon}{\delta} < \frac{\rho}{\lambda}, \tag{20}$$

where θ_r is the inclination angle of the exit of one column with its neighboring column at a distance δ. For the values given, the maximum of $\tan\theta_r$ is 7.5, corresponding to a large angle. Therefore, in principle, one can obtain the exact defocus value even for substantial surface roughness. In a forthcoming paper, we will show the theoretical limits of thickness and surface roughness measurements in terms of the highest attainable precision.

As shown above defocus circles are very useful to determine the surface profile at the *exit* plane. However, at the *entrance* plane, the heights of neighboring columns may also be different. This effect can also be observed in the Argand plot. A crystal structure in which the unit cell contains columns with a different relative displacement in the beam direction is shown in Fig. 7(a). The atoms in *b* columns are vertically displaced downwards compared to the *a* columns by half a lattice parameter. In Fig. 7(b), the Argand plot for *a* and *b* columns are shown. The neighboring dots for *a* and *b* columns contain the same number of atoms in the column. It is clear that the circles for *a* and *b* columns are relatively rotated. Moreover, by introducing potential eccentricity [20] on the *b* columns, i.e. correct for the deviation of the center of potential in the beam direction (which is equivalent to a shift of half a unit cell distance), the points of the *b* columns overlap with the *a* columns as shown in Fig. 7(c). One could argue whether the roughness of the entrance surface plays a role. However, surface roughness at the entrance plane only gives an arbitrary phase shift for the incoming wave of the atom column leading to a relative rotation in the Argand plot. The method presented here uses the fact that the atom column wave at the exit position is peaked at the column position. The peakiness in itself is not altered by a constant phase shift. Only in case the exit waves of neighboring columns become important, the relative phase shift between columns, which is affected by the roughness of the entrance face, can play a role. Moreover, once the surface roughness at the exit plane and the number of atoms in the columns are obtained, one automatically obtains the surface roughness at the entrance plane.

4. Conclusions

In this paper, the influence of neighboring columns is studied by means of the channelling theory. It is shown that for small defocus values, neighboring columns show negligible effect on the defocus circle whereas for larger defocus values the effect becomes more important. For large defocus values the column waves spread out very far and depend on the configuration of the atom columns. Therefore, the contributions from neighboring atom columns on the center column increase and become more difficult, or even impossible, to interpret. As explained in [6], in order to obtain the surface structure at atomic resolution, one can use the defocus circle to determine the zero-defocus point and next to calculate the exact defocus value for every atom column. From the results shown in this paper, it follows that large defocus values on the defocus circle cannot be used at all to find the zero-defocus point. The only suitable region on the defocus circle is the one close to the zero-defocus point. It has been shown that the useful defocus range is proportional to the distance between two columns and the resolution, and is inversely proportional to the wavelength. This range may be different for different atom types. In general, for the same number of atoms in an atom column, the heavier the atoms, the larger the useful defocus range, provided the thickness does not exceed half of the extinction distance. The only possible way we have investigated so far to find this range is to defocus the exit wave over a very large focal range and look for a stationary region where the defocus circle gives the largest curvature and the distances between neighboring focal points are the largest on this circle. From that curve one can then continue to obtain the exact defocus value for every atom column.

Acknowledgments

The authors are grateful to the Fund for Scientific Research—Flanders (Project no. G.0188.08) and the National Science Council of Taiwan (Project no. 96-2628-E-007-017-MY3).

References

[1] D. Van Dyck, M. Op de Beeck, A simple intuitive theory for electron diffraction, Ultramicroscopy 64 (1996) 99–107.
[2] K. Kambe, G. Lehmpfuhl, F. Fujimoto, Interpretation of electron channeling by the dynamical theory of electron diffraction, Zeitschrift für Naturforsch 29 (1974).
[3] F. Fujimoto, Periodicity of crystal structure images in electron microscopy with crystal thickness, Physica Status Solidi A 45 (1978) 99–106.
[4] A.J. den Dekker, S. Van Aert, A. van den Bos, D. Van Dyck, Maximum likelihood estimation of structure parameters from high resolution electron microscopy images. Part I. A theoretical framework, Ultramicroscopy 104 (2005) 83–106.
[5] S. Bals, S. Van Aert, G. Van Tendeloo, D. Avila-Brande, Statistical estimation of atomic positions from exit wave reconstruction with a precision in the picometer range, Physical Review Letters 96 (2006) 096106.
[6] A. Wang, F.R. Chen, S. Van Aert, D. Van Dyck, Direct structure inversion from exit waves. Part I: Theory and simulations, Ultramicroscopy 110 (2010) 527–534.
[7] C. Kisielowski, C.J.D. Hetherington, Y.C. Wang, R. Kilaas, M.A. O'Keefe, A. Thust, Imaging columns of the light elements carbon, nitrogen and oxygen with sub-Angstrom resolution, Ultramicroscopy 89 (2001) 243–263.
[8] P. Schiske, Image processing using additional statistical information about the object, in: Image Processing and Computer-aided Design in Electron Optics, Academic Press, London, 1973, pp. 82–90.
[9] W. Coene, A. Thust, D. Van Dyck, M. Op de Beeck, Maximum-likelihood method for focus-variation image reconstruction in high resolution transmission electron microscopy, Ultramicroscopy 64 (1996) 109–135.
[10] W.K. Hsieh, F.R. Chen, J.J. Kai, A.I. Kirkland, Resolution extension and exit wave reconstruction in complex hrem, Ultramicroscopy 98 (2004) 99–114.
[11] H. Lichte, Electron holography approaching atomic resolution, Ultramicroscopy 20 (1986) 293–304.
[12] J.M. Cowley, A.F. Moodie, Fourier Images: I—The point source, Proceedings of the Physical Society. Section B 70 (1957) 486–496.
[13] P. Geuens, D. Van Dyck, The S-state model: a work horse for HRTEM, Ultramicroscopy 93 (2002) 179–198.
[14] W. Sinkler, L.D. Marks, Dynamical direct methods for everyone, Ultramicroscopy 75 (1999) 251–268.
[15] R.W. Glaisher, A.E.C. Spargo, P.G. Self, Tuned voltage in zone-axis diffraction, Ultramicroscopy 32 (1990) 299–308.
[16] S. Van Aert, P. Geuens, D. Van Dyck, C. Kisielowski, J.R. Jinschek, Electron channelling based crystallography, Ultramicroscopy 107 (2007) 551–558.
[17] P. Geuens, J.H. Chen, A.J. den Dekker, D. Van Dyck, An analytic expression in closed form for the electron exit wave, Acta Crystallographica, Section A, 55 Supplement, Abstract P11.OE.002, 1999.
[18] P. Geuens, D. Van Dyck, The S-state model for electron channelling in high-resolution electron microscopy, Advances in Imaging and Electron Physics 136 (2005) 111–226.
[19] J.M. Cowley, A.F. Moodie, The scattering of electrons by atoms and crystals. I. A new theoretical approach, Acta Crystallographica 10 (1957) 609–619.
[20] D. Van Dyck, Fast computational procedures for the simulation of structure images in complex or disordered crystals: a new approach, Journal of Microscopy 119 (1980) 141–152.